THE JOURNAL OF BIOLOGICAL CHEMISTRY VOL. 288, NO. 13, pp. 9049–9057, March 29, 2013
© 2013 by The American Society for Biochemistry and Molecular Biology, Inc. Published in the U.S.A.

The Truncated C-terminal RNA Recognition Motif of TDP-43 Protein Plays a Key Role in Forming Proteinaceous Aggregates*[S]

Received for publication, November 20, 2012, and in revised form, January 23, 2013 Published, JBC Papers in Press, January 31, 2013, DOI 10.1074/jbc.M112.438564

Yi-Ting Wang[‡1], Pan-Hsien Kuo[‡1], Chien-Hao Chiang[‡§], Jhe-Ruei Liang[‡¶], Yun-Ru Chen[‖], Shuying Wang[‡‡], James C. K. Shen[‡], and Hanna S. Yuan[‡§§2]**

From the [‡]Institute of Molecular Biology, Academia Sinica, Taipei 11529, Taiwan, the [§]Institute of Bioinformatics and Structural Biology, National Tsing Hua University, Hsin Chu 30013, Taiwan, the [¶]Department of Life Sciences, Institute of Genome Sciences, National Yang-Ming University, Taipei 11221, Taiwan, the [‖]Genomics Research Center, Academia Sinica, Taipei 11529, Taiwan, the [**]Department of Microbiology and Immunology, College of Medicine, National Cheng Kung University, Tainan 70457, Taiwan, the [‡‡]Center of Infectious Disease and Signaling Research, National Cheng Kung University, Tainan 70457, Taiwan, and the [§§]Graduate Institute of Biochemistry and Molecular Biology, National Taiwan University, Taipei 10048, Taiwan

Background: TDP-43 forms aggregates in various neurodegenerative disorders.
Results: The C-terminal-truncated RRM2 of TDP-43 forms non-amyloid fibrils *in vitro* and plays a dominant role in forming inclusions *in vivo*.
Conclusion: The proteolytic cleavage of TDP-43 that removes the N-terminal dimerization domain may produce unassembled truncated RRM2 fragments for aggregation.
Significance: This result provides a new direction for the prevention and treatment of TDP-43-associated diseases.

TDP-43 is the major pathological protein identified in the cellular inclusions in amyotrophic lateral sclerosis and frontotemporal lobar degeneration. The pathogenic forms of TDP-43 are processed C-terminal fragments containing a truncated RNA-recognition motif (RRM2) and a glycine-rich region. Although extensive studies have focused on this protein, it remains unclear how the dimeric full-length TDP-43 is folded and assembled and how the processed C-terminal fragments are misfolded and aggregated. Here, using size-exclusion chromatography, pulldown assays, and small angle x-ray scattering, we show that the C-terminal-deleted TDP-43 without the glycine-rich tail is sufficient to form a head-to-head homodimer primarily via its N-terminal domain. The truncated RRM2, as well as two β-strands within the RRM2, form fibrils *in vitro* with a similar amyloid-negative staining property to those of TDP-43 pathogenic fibrils in diseases. In addition to the glycine-rich region, the truncated RRM2, but not the intact RRM2, plays a key role in forming cytoplasmic inclusions in neuronal cells. Our data thus suggest that the process that disrupts the dimeric structure, such as the proteolytic cleavage of TDP-43 within the RRM2 that removes the N-terminal dimerization domain, may produce unassembled truncated RRM2 fragments with abnormally exposed β-strands, which can oligomerize into high-order inclusions.

TDP-43 (TAR DNA-binding protein) is a DNA/RNA-binding protein, ubiquitously expressed in various tissues and highly conserved in mammals and invertebrates (1). TDP-43 has multiple cellular functions, such as serving as a transcriptional repressor for HIV-1 TAR sequences (2), mouse *acrv1* gene (3, 4), and human *Cdk6* gene (5) and functioning as a splicing factor promoting the pre-mRNA exon skipping or inclusion of cystic fibrosis transmembrane conductance regulator (6, 7), apolipoprotein A-II (8), and survival of motor neuron (SMN2) (9). TDP-43 has also been reported to play a role in mRNA transportation (10), mRNA translation regulation (11–13), micro-RNA processing (14), and is associated with stress granules (15, 16).

Apart from its various functions in the nucleus and cytoplasm, TDP-43 has been the focus of extensive studies since it was identified as the major pathological protein in the cellular inclusions in amyotrophic lateral sclerosis and frontotemporal lobar degeneration (17, 18). The pathology of TDP-43 has also been characterized in various neurodegenerative disorders, including Alzheimer, Parkinson, and Huntington diseases (19–21). The disease form of TDP-43 is hyperphosphorylated, ubiquitinated, and proteolytically cleaved into C-terminal fragments (CTFs)[3] of ~25 kDa. The pathogenic TDP-43 inclusions comprise granular and filamentous structures, but they cannot be stained by the amyloid-binding dye, such as thioflavin T and Congo red (22, 23). Recent studies further showed that the 25-kDa CTFs of TDP-43 form insoluble cytoplasmic aggregates (24) and toxic inclusions in cell lines (25, 26). Moreover, the amount of TDP-43 CTFs that accumulated in a cell correlated with disease progression in transgenic mice, suggesting that the

* This work was supported by research grants from Academia Sinica (to H. Y. and J. C. K. S.) and the National Science Council (Taiwan) (to H. Y. and J. C. K. S.).
⌘ *Author's Choice*—Final version full access.
[S] This article contains supplemental Fig. 1.
[1] Both authors contributed equally to this work.
[2] To whom correspondence should be addressed: Inst. of Molecular Biology, Academia Sinica, Taipei 11529, Taiwan. Tel.: 886-2-27884151; Fax: 886-2-27826085; E-mail: hanna@sinica.edu.tw.

[3] The abbreviations used are: CTF, C-terminal fragment; NTD, N-terminal domain; RRM, RNA recognition motif; SAXS, small angle x-ray scattering; PDB, Protein Data Bank; ThT, thioflavin T; tRRM2, truncated RRM2.

accumulation of aberrant TDP-43 CTFs may lead to neuronal dysfunction (27).

The domain structure of TDP-43 is similar to the heterogeneous nuclear ribonucleoprotein (28), consisting of an N-terminal domain (NTD) and two tandem RNA recognition motifs (RRM1 and RRM2), followed by a C-terminal glycine-rich region (Gly) (see Fig. 1*A*). TDP-43 forms homodimers, and the RNA recognition motifs are involved in DNA and RNA binding (29–31). Previous studies in TDP-43 proteinopathies and aggregation mainly focused on the glycine-rich region because most of the TDP-43 mutations in amyotrophic lateral sclerosis are located in this region. Indeed, it has been shown that the amyotrophic lateral sclerosis-linked TDP-43 mutations at the glycine-rich region are more prone to forming aggregates with increased toxicity (32, 33), and a small peptide (residues 287–332) in this region can form twisted fibrils *in vitro* (34).

However, not much is known about the involvement of the TDP-43 RRM2 domain in protein aggregation, although previous cell line studies suggest that the C-terminal part of RRM2 is required for aggregation (26, 35, 36). The crystal structure of TDP-43 RRM2 shows that it has a fold composed of two α-helices packed against a five-stranded β-sheet with a $\beta2$-$\beta3$-$\beta1$-$\beta5$-$\beta4$ topology (31). The pathogenic C-terminal fragments of TDP-43 are likely generated by the processing at the sites of Arg-208 (residues 209–414) (24) or Asp-219 (residues 220–414) (37–39). The processing of TDP-43 at these sites removes the $\beta1$-strand and $\alpha1$-helix in RRM2 and thus may disrupt the folding of this domain. Because a broad range of amyloidoses and neurodegenerative diseases are initiated by protein misfolding or unfolding (40, 41), whether RRM2 plays a central role in TDP-43 aggregation poses an intriguing question.

To understand how the functional TDP-43 is folded and how the processed TDP-43 is aggregated, we used biochemical and biophysical approaches, including GST pulldown assays and small angle x-ray scattering (SAXS), to study the domain assembly of TDP-43. We found that TDP-43 formed a homodimer via its N-terminal domain, and the RRM2 domain was flanked outward. The truncated RRM2 formed fibrils *in vitro* and played a key role in forming inclusions *in vivo*. We therefore propose a model whereby the processing of a dimeric TDP-43 leads to protein disassembly and misfolding, resulting in CTF inclusions.

EXPERIMENTAL PROCEDURES

Cloning, Expression, and Purification—The cDNA of NTD-RRM12 (residues 1–265), NTD (1–100), RRM1 (101–191), and RRM2 (192–265) was amplified from the human *TARDBP* gene and inserted into the BamHI/HindIII sites in the pQE30 vector (Qiagen) for the expression of the N-terminal His-tagged recombinant proteins. The cDNA of NTD-RRM12 was cloned into the BamHI/NotI sites of the pGEX-4T-1 vector (GE Healthcare) for the expression of the N-terminal glutathione *S*-transferase tagged NTD-RRM12 (GST-NTD-RRM12). The plasmids were transformed into the *Escherichia coli* M15 strain cultured in LB medium supplemented with 100 μg/ml ampicillin for protein expression. The bacteria were cultured at 37 °C for 4 h and then induced by 0.8 mM isopropyl 1-thio-β-D-galactopyranoside at 18 °C for 22 h. The cell extracts containing the His-tagged NTD-RRM12 were applied to a nickel-nitrilotriacetic acid affinity column (Qiagen) equilibrated with 100 mM NaCl, 10 mM β-mercaptoethanol, and 50 mM phosphate buffer at pH 7.5. The protein samples were further purified by a HiTrap heparin column (GE Healthcare) followed by a Superdex 200 gel filtration column (GE Healthcare). The GST-NTD-RRM12 fusion protein was purified by glutathione-Sepharose beads (GE Healthcare).

GST Pulldown Assays—The GST-tagged NTD-RRM12 protein sample in 10 mM β-mercaptoethanol, 100 mM NaCl, and 50 mM phosphate buffer (pH 7.5) was incubated with glutathione-Sepharose beads (GE Healthcare) for 1 h at 4 °C before it was mixed overnight with the His-tagged NTD-RRM12, NTD, RRM1, and RRM2, respectively. The beads were washed extensively to remove nonspecific binding proteins and then eluted with buffer containing 10 mM reduced glutathione. The eluted samples were collected and separated using 12.5% SDS-PAGE and transferred onto a PVDF membrane for Western blotting. GST-tagged NTD-RRM12 and His-tagged TDP-43 proteins were probed with anti-GST and anti-His antibodies (Novagen), respectively. Protein bands were detected by chemiluminescence with an ECL luminescence kit (Amersham Biosciences) and visualized by luminescence image analyzer Fuji LAS-1000plus (Fujifilm).

SAXS—Fresh protein samples collected from the gel filtration chromatography were used for SAXS in a buffer of 150 mM NaCl, 10 mM β-mercaptoethanol and 50 mM phosphate at pH 7.6. Protein solutions were loaded into a 3-mm mica 4-loading rocking cell with kapton windows. The SAXS data were recorded at BL23A, National Synchrotron Radiation Research Center, Hsinchu, Taiwan. The sample-to-detector distance was 2.4 m for NTD-RRM12 using x-ray of a wavelength of 1.03 Å (12 keV) and 2.9 m for GST-NTD-RRM12 of a wavelength of 0.88 Å (14 keV) to cover the scattering vector (q) ranging from 0.007 to 0.31 $Å^{-1}$, where $q = 4\pi\sin\theta/\lambda$. The q axis was calibrated by the scattering pattern of silver-behenate salt. The exposure time (100 to 300 s) was optimized so as to exclude the interference of protein aggregations resulting from radiation damage.

A series of scattering curves were collected with various concentrations of protein samples ranged 2~5 mg/ml. SAXS data were analyzed by the ATSAS program suite (version 2.4) (42). Composite scattering curves were scaled and merged by program PRIMUS (43). Radius of gyration was initially computed by the Guinier approximation as implemented in PRIMUS with the criteria of $qR_g < 1.3$ and subsequently calculated by the distance distribution functions $P(r)$. The maximum intramolecular distance (D_{max}) and $P(r)$ function were determined by GNOM (44). The R_g calculated from the Guinier plots were in consistent with the values derived from the $P(r)$ function (supplemental Fig. 1). For *ab initio* low resolution structures, molecular shapes were computed with the program DAMMIN (45) and GASBOR (46) with default settings and a 2-fold symmetry. Both calculations generated similar molecular envelopes. The calculated dummy atom model curve fitted well with the experimental scattering curves (data not shown). Due to the lacking of the structure of NTD, rigid-body modeling of an

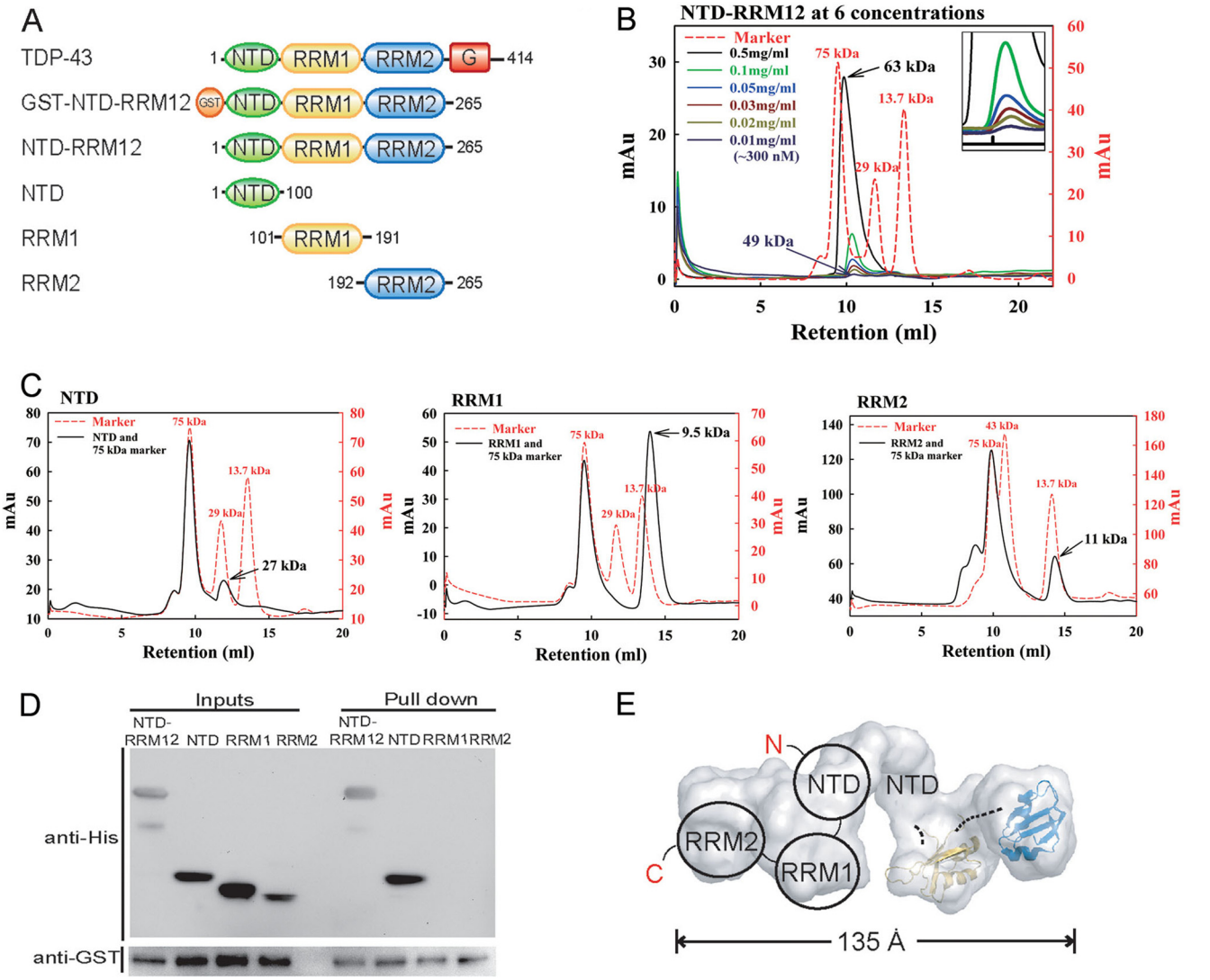

FIGURE 1. **TDP-43 forms an elongated homodimer via its N-terminal domain.** *A*, TDP-43 has four domains: an NTD (*N*), two tandem RNA recognition motifs (RRM1 and RRM2), and a C-terminal glycine-rich (*G*) region (*C*). *B*, gel filtration profiles of NTD-RRM12 show that NTD-RRM12 (0.5 mg/ml) was a homodimer with an estimated molecular mass of 63 kDa (calculated molecular mass of NTD-RRM12 monomer, 31,860 Da). At low concentrations, NDT-RRM12 dimers dissociated partially into monomers with shifted peaks. The buffer solution was 50 mM $NaHPO_4$, 100 mM NaCl, and 10 mM β-mercaptoethanol (pH 7.5). *C*, RRM1 (1 mg/ml, calculated molecular mass, 12,396 Da) and RRM2 (1 mg/ml, calculated molecular mass, 10,169 Da) were monomers with molecular masses of 9.5 and 11 kDa, respectively. *D*, GST pulldown assays show that the GST-NTD-RRM12 could pull down the His-tagged NTD-RRM12 and NTD, but not RRM1 and RRM2. *E*, the *ab initio* envelope of NTD-RRM12 generated from SAXS data reveals the elongated structure with three domains in each subunit of the dimer. The domain structures of RRM1 and RRM2 (PDB codes 2CQG and 3D2W) were manually fitted into the envelope.

overall low-resolution structure cannot be performed. The available NMR structure of RRM1 and crystal structures of RRM2 and GST (PDB codes 2CQG, 3D2W, and 1UA5) were manually placed into the SAXS envelope.

In Vitro Fibril Formation and EM—Peptides of TDP-43 fragments, truncated RRM2 (residues 208 to 265), β1(RKVFVGR), β2 (MDVFIPKPF), β3 (RAFAFVT), β4 (GEDLII), β5 (ISVHISN), and D1s (FGAFSIN) were synthesized (MDBio, Inc.). Peptide solutions in 20 mM phosphate buffer (pH 7) were centrifuged for 5 min at 16,100 $\times$ *g* and filtered through a 0.22-μm filter (Millipore) to remove insoluble material. The protein samples were set aside at room temperature, and fibrils appeared in 2 to 3 weeks. The fibril solution (2 μl) was placed on 300-square-mesh carbon-coated, glow-discharged grids (Electron Microscopy Science). The grid was washed six times with water before staining with 0.75% uranyl formate for 1 min. After air drying, the peptide fibrils on the grid were examined by transmission electron microscopy Tecnai G2 Spirit TWIN (FEI Company) at 120 kV.

Circular Dichroism (CD) Measurements—All far-UV CD spectra were recorded on the Aviv circular dichroism spectrometer MODEL 400, using a quartz cell with 1-mm path length. Protein solutions were diluted with 50 mM phosphate buffer (pH 7.5) to give the same protein concentrations of 30 μM in a total volume of 300 μl. Each spectrum was taken at a specific temperature with three scans ranging from 260 to 195 nm. The final spectra were represented by mean residue ellipticity (θ) in deg·cm^2·dmol^{-1}. Thermal denaturation experiments were carried out by raising the temperature from 25 to 85 °C in 1-degree intervals with a 0.5-min equilibration time at

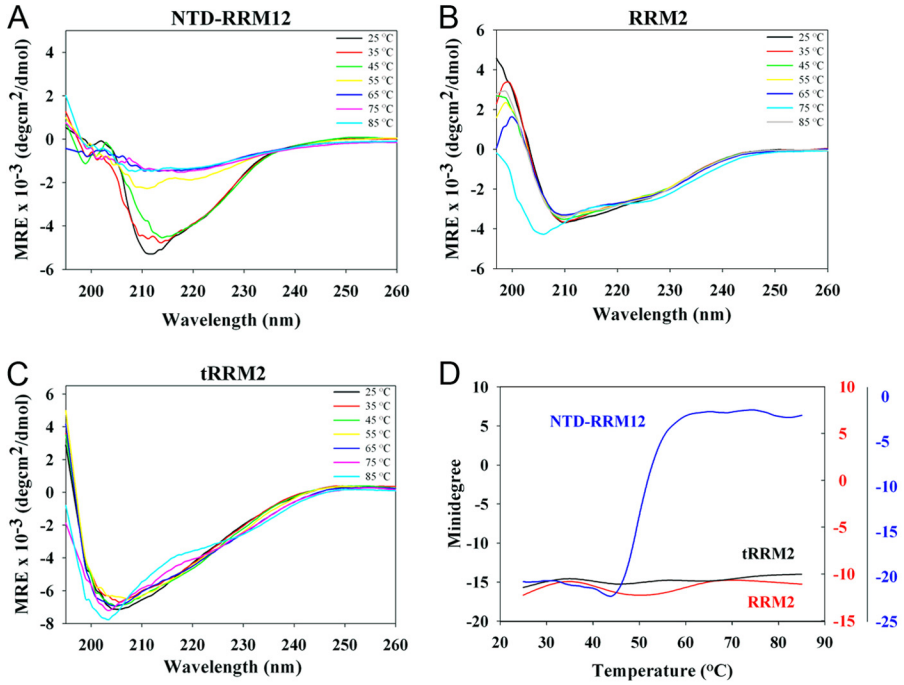

FIGURE 2. **The TDP-43 RRM2 domain and the truncated tRRM2 domain were resistant to thermal denaturation.** *A–C*, thermal denaturation of NTD-RRM12 (residues 1–265), RRM2 (residues 192–265), and tRRM2 (residues 208–265) was assayed by circular dichroism from 25 to 85 °C in 50 mM phosphate buffer at pH 7.5. *D*, the melting point was 50.5 °C for NTD-RRM12, monitored at a wavelength of 218 nm. RRM2 and tRRM2 were not melted at temperature as high as 85 °C as monitored at a wavelength of 208 nm.

each temperature. The structural changes were monitored at a wavelength of 208 nm for NTD-RRM12 and 218 nm for RRM2 and truncated RRM2 (tRRM2).

Thioflavin T (ThT) Binding Assays and Anti-amyloid Fiber Dot Blotting—The fluorescence of fibril samples in the presence of 100 μM thioflavin T was measured in 20 mM phosphate buffer at pH 7. The ThT solution was freshly prepared and filtered through a 0.22-μm filter before use. The fibril solutions and ThT solution were mixed in a 1:1 ratio for 5 min at room temperature. Samples were excited at 442 nm, and the fluorescence emission intensity was recorded from 455 to 600 nm using a Carv Eclipse Fluorescence Spectrophotometer (Varian).

Aβ fibrils used for the positive control were prepared as described previously (47). TDP-43 fibril samples and Aβ fibrils (2 μl) were applied to a nitrocellulose membrane and allowed to air dry. Nonspecific binding was blocked by incubation with 5% nonfat milk in TBST solution at room temperature for 30 min. After a brief wash with the TBST buffer of 50 mM Tris, 150 mM NaCl, and 0.05% Tween 20 (pH 7.6), the membrane was dipped into 5% milk-TBST with anti-amyloid fibril OC antibody (Millipore) and incubated with gentle shaking for 1 h, followed by washing with TBST. Blots were then incubated with anti-rabbit antibody (Amersham Biosciences) for 1 h, washed three times with TBST, developed by the ECL luminescence kit t8 (Amersham Biosciences), and visualized using the luminescence image analyzer Fuji LAS-1000plus (Fujifilm).

Cell Transfection—The full-length cDNA were cloned into XhoI/XbaI sites of expression vector pEGFPC1 (Clontech) using the following primers: 5′-AGATCTCGAGCGTCTGAATATATTCGGGTAACC-3′ and 5′-TTATCTAGACTACATTCCCCAGCCAGAA-3′ (XhoI and XbaI restriction sites are *underlined*). The different TDP-43-truncated forms, RRM2-GFP (192–265), RRM2-G-GFP (192–414), tRRM2-GFP (208–265) and tRRM2-G-GFP (208–414), and G-GFP (266–414) were generated using two of the following primers: 192 (5′-GTACTCGAGATAAAGTGTTTGTGGGGCGCT-3′), 265 (5′-CATTCTAGAATTGTGCTTAGGTTCGGCAT-3′), 266 (5′-GTACTCGAGTAAGCAATAGACAGTTAGAAAGAAG-3′), and 414 (5′-CATTCTAGACTACATTCCCCAGCCAGAA-3′). All of the plasmid products were checked by DNA sequencing.

The N2A cells were maintained in minimum essential medium supplemented with 10% FBS, 1% penicillin/streptomycin, and sodium pyruvate at 37 °C. The cells were subcultured every 2 days and seeded on coverslips in six-well plates that were coated overnight with 0.5% gelatin. A total of 4×10^5 cells on the coverslip were transfected using PolyJet^{TM} (SignaGen) according to the manufacturer's instructions. The transfected cells were then fixed with 4% (w/v) paraformaldehyde in PBS for 15 min and then permeated with 0.1% (w/v) Triton X-100 in PBS for 5 min. After permeabilization, the fixed cells were blocked with 5% (w/v) donkey serum in PBST for 1 h and then incubated with TDP-43 rabbit polyclonal antibody (1:500; Protein Tech) in PBST at 4 °C overnight. After three washes with PBST, the cells were incubated with 4′,6-diamidino-2-phenylindole (DAPI) (1:500; Sigma) to detect the DNA in the nucleus and also incubated with the secondary antibody 488-conjugated goat anti-rabbit IgG (1:500; Molecular Probes) for 1 h. After three PBST washes, the coverslips were mounted with VECTASHIELD Mounting Medium (Vector Laboratories). The cells were photographed along the *z* axis using a Zeiss laser confocal microscope (LSM510 Meta). After photographing, the number of cells with a GFP-positive signal was calculated by Laser Scanning Microscopy ZEN 2009 (Carl Zeiss Microscopy).

The number of cells with an aggregation-positive signal was normalized using the GFP-positive cell number. The different aggregation ratios were analyzed by Student's *t* test.

RESULTS

TDP-43 Forms an Elongated Homodimer via Its N-terminal Domain—To reveal how TDP-43 is folded as a functional protein, a number of N-terminal His-tagged TDP-43 constructs were expressed in *Escherichia coli* and purified to a high homogeneity, including the Gly-rich region truncated TDP-43 (named NTD-RRM12, residues 1–265), NTD (1–100), RRM1 (101–181), and RRM2 (192–285). The Gly-rich region was removed in NTD-RRM12 because this random coil region was unstable and degraded with time (Fig. 1*A*). The NTD-RRM12 had a molecular mass of ~63 kDa as estimated by size exclusion chromatography (Fig. 1*B*) and dynamic light scattering (data not shown) close to the calculated molecular mass of a homodimer (63.72 kDa). The estimated molecular masses of NTD-RRM12 were decreased with reduced protein concentrations: 62 kDa (100% dimers) in 0.5 mg/ml and 49 kDa (54% dimers) in 0.01 mg/ml (~300 nM) (see Fig. 1*B*). This result suggests that NTD-RRM12 is a stable homodimer with a dissociation constant of ~300 nM.

The NTD also formed a homodimer with an estimated molecular mass of 27 kDa; nevertheless, RRM1 and RRM2 were monomers with estimated molecular masses of 9.5 and 11 kDa by size exclusion chromatography (Fig. 1*C*). GST pulldown assays further revealed that the GST-tagged NTD-RRM12 was capable of pulling down the His-tagged NTD-RRM12 and NTD, but not RRM1 or RRM2 (Fig. 1*D*). Taken together, these results suggest that NTD-RRM12 forms a homodimer mainly via NTD.

To clarify the domain arrangement of TDP-43, SAXS was performed to obtain the *ab initio* molecular envelope of NTD-RRM12. The measurements revealed an elongated molecular envelope of a size of 135 × 65 × 60 Å^3 with three bulged regions in each half of the dimeric envelope (Fig. 1*E*). The three bulged regions could be manually fitted with the three globular domains of TDP-43, *i.e.* NTD, RRM1 (PDB code 2CQG), and RRM2 (PDB code 3D2W). SAXS analysis was also performed for the N-terminal GST-tagged NTD-RRM12 (supplemental Fig. 1). Superimposition of the two envelopes revealed an additional GST domain located next to the NTD, thereby confirming that TDP-43 formed an elongated dimer primarily via the NTD, with the RRM2 domain flanked at two sides.

Truncated RRM2 Forms Amyloid-negative Fibrils—Based on the SAXS model of TDP-43, the NTD is important for dimerization. Therefore, removal of the N-terminal part of TDP-43 by the processing at Arg-208 and Asp-219 may disrupt TDP-43 dimer formation and reveal a surface in RRM2 necessary for protein aggregation. To examine whether the truncated RRM2 may participate in aggregate formation, tRRM2 (residues 208–265), was synthesized for thermal denaturation and fibril formation studies. In contrast to the dimeric NTD-RRM12 that had a melting point of 50.5 °C, RRM2 and tRRM2 had unusual thermal stability and retained secondary structures up to 85 °C as monitored by circular dichroism (Fig. 2). This result suggests that the RRM2 and tRRM2 formed a highly

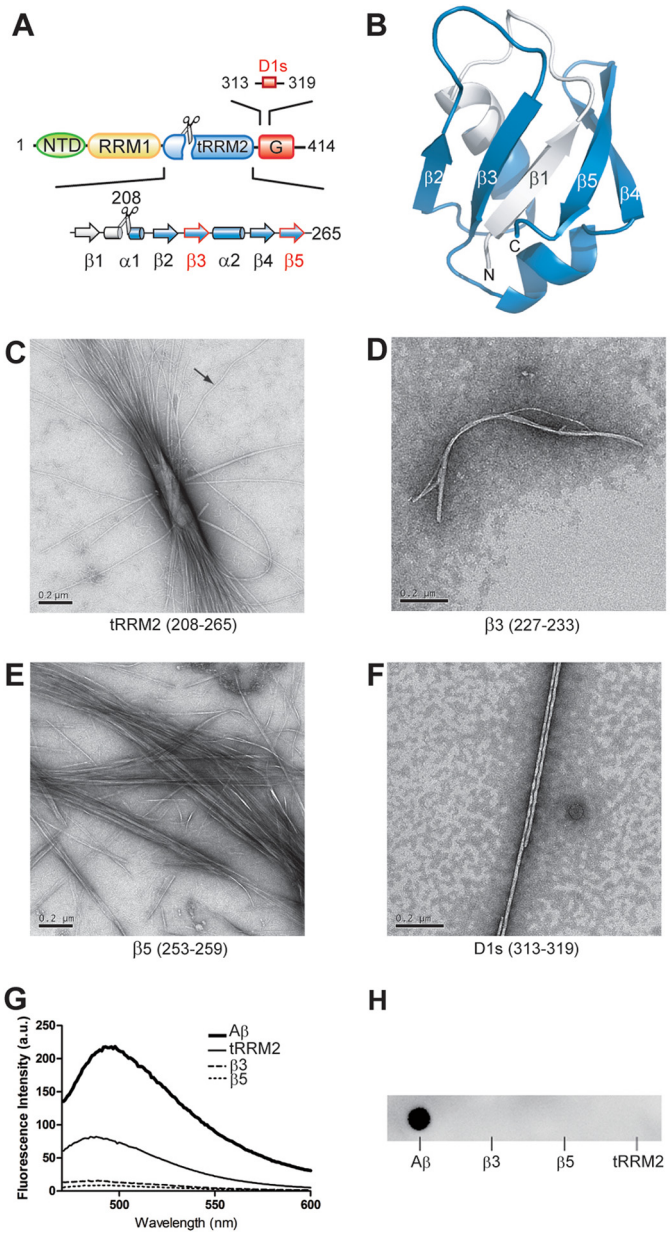

FIGURE 3. **The truncated RRM2 domain of TDP-43 forms fibrils.** *A*, the TDP-43 protein is processed at Arg-208 and Asp-219 (indicated by *scissors*) within RRM2 to generate the pathogenic C-terminal fragments. *B*, the crystal structure of the RRM2 domain (PDB code 3D2W) reveals a five-stranded β-sheet packed against two α-helices. The C-terminal pathogenic fragment (208–265) is displayed in *blue*, and the N-terminal cleaved region (192–207) is displayed in *gray*. *C*, the truncated tRRM2 forms fibril bundles with a fiber diameter of 10 nm. *D* and *E*, the β3 (residues 227–233) and β5 (residues 253–259) form thin fibrils with a diameter of 5–7 nm. *F*, the D1s peptide in the Gly-rich region (residues 313–319) forms twisted straight fibrils with a diameter of ~11 nm. *G*, ThT fluorescence assays showed that Aβ (amyloid β-peptides 1–40) fibrils (~0.3 mg/ml) had a fluorescence emission signal, whereas β3 and β5 fibrils (~2.5 mg/ml) had no signal, and tRRM2 fibrils had a weak signal, indicting a weak binding to the ThT dyes (100 μM). *H*, Aβ, β3 and β5, and tRRM2 fibril solutions were dipped onto a nitrocellulose membrane to perform dot blotting assays. The samples were probed by amyloid fiber structure-specific antibody, OC. Only the Aβ sample can be recognized by anti-OC, whereas β3, β5, and tRRM2 fibrils cannot be blotted by OC antibodies. Fluorescence intensity is given in arbitrary units (*A.U.*).

stable structure resistant to thermal denaturation, a feature that has been observed in prion proteins (48).

The tRRM2 peptides were further incubated in phosphate buffers at room temperature for 3 weeks. As revealed by nega-

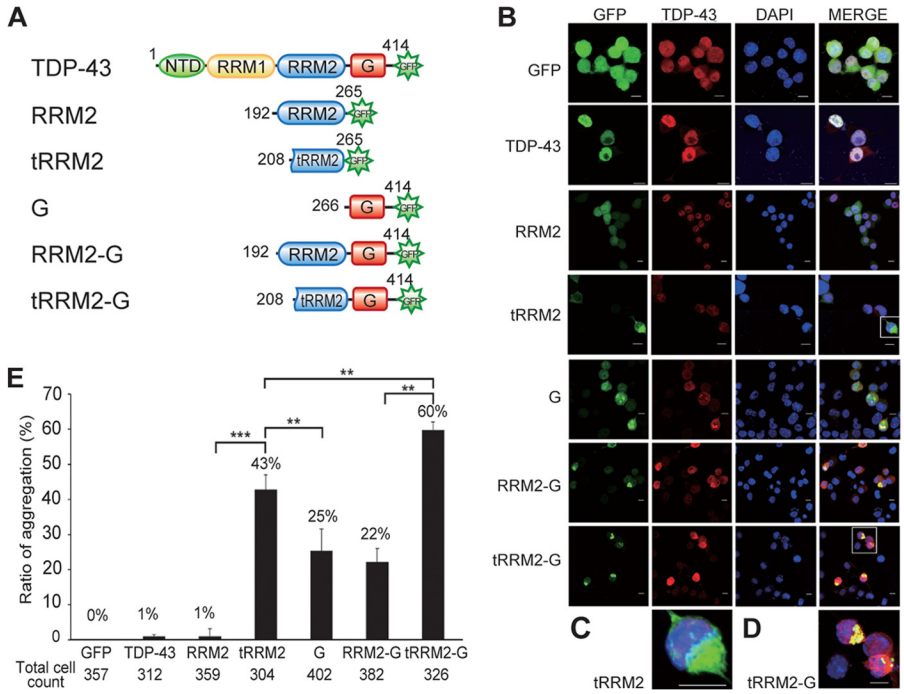

FIGURE 4. **The truncated tRRM2 domain and Gly-rich region in TDP-43 form cytoplasmic inclusions in neuronal cells.** *A*, different constructs were made for the expression of the GFP-fused TDP-43 fragments. *B*, confocal micrographs of Neuro2a cells expressing various GFP-tagged TDP-43 fragments. The N2A cells expressing GFP, full-length TDP-43 and RRM2 exhibited diffuse patterns of expression whereas the cells expressing RRM2-G, tRRM2-G, tRRM2, and G had inclusions in the cytoplasm. The *scale bar* is 10 μm. *C*, the magnified view of the inclusions in the cells expressing tRRM2 (*green* inclusions as RRM2 domain was only weakly stained with TDP-43 antibodies). *D*, magnified view of the inclusions in the cells expressing tRRM2-G (*yellow* inclusions as merged from *green* GFP and *red* TDP-43). The inclusions were located in the cytoplasm right above the nucleus as further confirmed by three-dimensional sections (data not shown). *E*, the ratio of cells with aggregates verses without was calculated for a total of 300–400 cells per construct.

tive stain electron microscopy, tRRM2 formed long well structured three-dimensional fibril bundles (>2 μm) with a fibril diameter of ~10 nm, similar in size to the ~11-nm diameter of the pathogenic TDP-43 fibrils (22) (Fig. 3). To further test which β strand in RRM2 might contribute to fibril formation, each β strand of RRM2, including β1 (RKVFVGR), β2 (MDVFIPKPF), β3 (RAFAFVT), β4 (GEDLII), and β5 (ISNHISN), was synthesized for fibril formation studies. A 40-amino acid peptide D1 in the Gly-rich region of TDP-43 has been shown to form fibrils in phosphate buffers (34). A shorter D1s peptide (^{313}FGAFSIN^{319}) was thus synthesized for a positive control, based on the prediction of amyloidogenic regions using WALTZ (49). After incubation in the phosphate buffer for 2 weeks, two β-strands, β3 and β5, formed long straight sheet-like fibrils with a diameter of 5 to 7 nm (Fig. 3, *D* and *E*). In contrast, β1, β2, and β5 did not form fibrils, whereas D1s formed thicker and twisted fibrils with a diameter of ~11 nm (Fig. 3*F*).

The pathogenic TDP-43 fibrils extracted from patient brains have a unique feature: they cannot be stained by amyloid-detecting dyes, such as ThT (50). To determine whether the peptide fibrils shared similar properties to those of pathogenic fibrils, the filamentous solutions of tRRM2, β3, and β5 were tested for the binding of ThT and the structure-specific anti-amyloid fibril OC antibodies, using the Aβ amyloid fibril as a positive control (Fig. 3, *G* and *H*) (51). In contrast to Aβ amyloid fibrils, tRRM2, β3, and β5 fibrils could not be stained, or were only weakly stained, by ThT, and none of them was immunoreactive for amyloid-specific antibodies, suggesting that these fibrils share similar amyloid-negative properties with those pathogenic TDP-43 inclusions.

Truncated RRM2 Plays a Key Role in Forming Cytoplasmic Inclusions—To corroborate the finding that the truncated RRM2 might play an important role in inclusion formation, the GFP-tagged TDP-43 fragments containing either RRM2 or tRRM2 with or without a Gly-rich region, were expressed in mouse neuroblastoma N2a cells (Fig. 4). The expression of each protein in N2a cells was verified by Western blotting (data not shown). In addition to the GFP control, the full-length TDP-43 (1–414) and RRM2 (192–265) were expressed in a diffuse pattern in cells. In contrast, cytoplasmic inclusions were observed in the cells expressing RRM2-G (192–414), tRRM2-G (208–414), tRRM2 (208–265), and G (266–414). The ratio of cells with inclusions *versus* those without was calculated based on a total of 300 to 400 cells. The full-length TDP-43 (1%) and RRM2 (1%) aggregated only at low levels. The tRRM2 (43%) and Gly-rich region (25%) alone were capable of forming inclusions, and combining the two regions, the pathogenic fragment tRRM2-G had the highest aggregation ratio (60%). Comparing the ratio of RRM2 (1%) *versus* tRRM2 (43%), as well as RRM2-G (22%) *versus* tRRM2-G (60%) clearly demonstrated that the truncated RRM2 significantly increased the ratio of inclusions by 43 and three times, respectively, when compared with those with the intact RRM2. These results suggest that both the tRRM2 and Gly-rich regions contribute to inclusion formation with the truncated RRM2 domain likely playing a primary role.

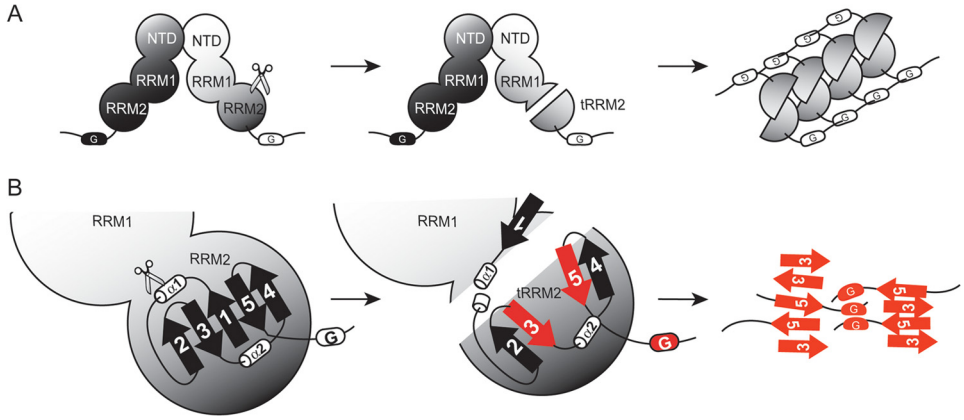

FIGURE 5. **Misfolding of TDP-43 by the processing within the RRM2 domain.** *A*, the proteolytic processing within the RRM2 disrupts the dimeric structure of TDP-43 and produces truncated RRM2 fragments that can oligomerize into high-order inclusions. *B*, the truncated RRM2 fragments without the β1 strand located in the center of the β-sheet are misfolded with abnormally exposed β3 and β5 strands and Gly-rich region that may be further assembled into oligomers.

DISCUSSION

Based on this study, we conclude that TDP-43 functions as an elongated homodimer with a head-to-head arrangement primarily through the interactions between regions of the NTD. We cannot exclude the possibility that the C-terminal glycine-rich region may contribute to or interfere with dimerization; yet, our data here show that TDP-43 without the glycine-rich C-terminal tail is sufficient in forming a stable homodimer.

TDP-43 forms dimers in the absence of bound RNA, a property that is different from the heterogeneous nuclear ribonucleoprotein superfamily protein heterogeneous nuclear ribonucleoprotein A1, which forms dimers only when bound with single-stranded DNA or RNA (52). Nevertheless, it is possible that TDP-43 may form a more stable dimer with bound RNA. Moreover, TDP-43 exhibits a novel domain organization that has not been observed in proteins with tandem RRM domains (53). TDP-43 binds to UG repeats up to a length of 15 nucleotides (54). As the binding length of a single RRM domain ranges from two to eight nucleotides (53), the dimeric conformation of TDP-43 may be critical for its recognition of RNA with long UG repeats, which are preferentially expressed in brain (55).

The proteolytic cleavage of TDP-43 within RRM2 removes the NTD for dimerization and therefore disrupts the dimeric assembly. The glycine-rich region in the processed TDP-43 forms aggregates in cultured neuronal cells and *in vitro* (24, 34, 56, 57). Here, we further narrow down the fibrogenesis region to a short peptide region (residues 313–319). Apart from the glycine-rich region, we show here that the truncated RRM2, but not the intact RRM2, is also capable of forming fibrils *in vivo* and *in vitro*. Two β-strands within RRM2, β3 and β5, are particularly prone to fibril formation, forming two-dimensional sheet-like fibrils, in a way resembling that of the protofilaments of amyloid fibrils (58). The truncated RRM2 are packed into long thicker three-dimensional fibril bundles, indicating that not only the aggregation-prone segments are important but also the overall three-dimensional structure of RRM2 is critical for the formation of large filaments.

The proteolytic processing in RRM2 removes the β1 strand located in the center of the β-sheet and generates a highly stable misfolded truncated RRM2 with abnormally exposed β3 and β5 strands (Fig. 5). It is possible that the process that disrupts the dimeric structure, such as the proteolytic processing within the RRM2 domain (24, 37–39), may lead to protein disassembly and misfolding. Environmental changes, such as oxidative stress (59), RNA depletion (60), or TDP-43 overexpression may also induce protein disassembly. The unassembled misfolded TDP-43 may form β-structures via these abnormally exposed β-strands in the RRM2 domain and potentially in the Gly-rich region similar to those of amyloid cross-β-structures (41). Nevertheless, the aggregated β-structures of TDP-43 have a unique structure that cannot be stained by amyloid-specific dyes or antibodies. Our study here thus provides a molecular foundation to understand how TDP-43 is folded into a functional homodimer and suggests a plausible mechanism to explain how this protein is misfolded and linked to TDP-43 proteinopathies.

Acknowledgments—We thank the IMB Electron Microscope Facility for technical assistance with the EM, and the BL-23A beamline in the National Synchrotron Radiation Research Center for SAXS data collection and analysis.

REFERENCES

1. Lee, E. B., Lee, V. M., and Trojanowski, J. Q. (2012) Gains or losses: molecular mechanisms of TDP43-mediated neurodegeneration. *Nat. Rev. Neurosci.* **13,** 38–50
2. Ou, S. H., Wu, F., Harrich, D., García-Martínez, L. F., and Gaynor, R. B. (1995) Cloning and characterization of a novel cellular protein, TDP-43, that binds to human immunodeficiency virus type 1 TAR DNA sequence motifs. *J. Virol.* **69,** 3584–3596
3. Abhyankar, M. M., Urekar, C., and Reddi, P. P. (2007) A novel CpG-free vertebrate insulator silences the testis-specific SP-10 gene in somatic tissues: role for TDP-43 in insulator function. *J. Biol. Chem.* **282,** 36143–36154
4. Lalmansingh, A. S., Urekar, C. J., and Reddi, P. P. (2011) TDP-43 is a transcriptional repressor: the testis-specific mouse acrv1 gene is a TDP-43 target *in vivo*. *J. Biol. Chem.* **286,** 10970–10982
5. Ayala, Y. M., Misteli, T., and Baralle, F. E. (2008) TDP-43 regulates retinoblastoma protein phosphorylation through the repression of cyclin-dependent kinase 6 expression. *Proc. Natl. Acad. Sci. U.S.A.* **105,** 3785–3789
6. Buratti, E., Dörk, T., Zuccato, E., Pagani, F., Romano, M., and Baralle, F. E. (2001) Nuclear factor TDP-43 and SR proteins promote *in vitro* and *in vivo* CFTR exon 9 skipping. *EMBO J.* **20,** 1774–1784
7. Buratti, E., Brindisi, A., Giombi, M., Tisminetzky, S., Ayala, Y. M., and

Baralle, F. E. (2005) TDP-43 binds heterogeneous nuclear ribonucleoprotein A/B through its C-terminal tail: an important region for the inhibition of cystic fibrosis transmembrane conductance regulator exon 9 splicing. *J. Biol. Chem.* **280,** 37572–37584
8. Mercado, P. A., Ayala, Y. M., Romano, M., Buratti, E., and Baralle, F. E. (2005) Depletion of TDP 43 overrides the need for exonic and intronic splicing enhancers in the human apoA-II gene. *Nucleic Acids Res.* **33,** 6000–6010
9. Bose, J. K., Wang, I. F., Hung, L., Tarn, W. Y., and Shen, C. K. (2008) TDP-43 overexpression enhances exon 7 inclusion during the survival of motor neuron pre-mRNA splicing. *J. Biol. Chem.* **283,** 28852–28859
10. Wang, I. F., Wu, L. S., Chang, H. Y., and Shen, C. K. (2008) TDP-43, the signature protein of FTLD-U, is a neuronal activity-responsive factor. *J. Neurochem.* **105,** 797–806
11. Ayala, Y. M., De Conti, L., Avendaño-Vázquez, S. E., Dhir, A., Romano, M., D'Ambrogio, A., Tollervey, J., Ule, J., Baralle, M., Buratti, E., and Baralle, F. E. (2011) TDP-43 regulates its mRNA levels through a negative feedback loop. *EMBO J.* **30,** 277–288
12. Fiesel, F. C., Voigt, A., Weber, S. S., Van den Haute, C., Waldenmaier, A., Görner, K., Walter, M., Anderson, M. L., Kern, J. V., Rasse, T. M., Schmidt, T., Springer, W., Kirchner, R., Bonin, M., Neumann, M., Baekelandt, V., Alunni-Fabbroni, M., Schulz, J. B., and Kahle, P. J. (2010) Knockdown of transactive response DNA-binding protein (TDP-43) downregulates histone deacetylase 6. *EMBO J.* **29,** 209–221
13. Strong, M. J., Volkening, K., Hammond, R., Yang, W., Strong, W., Leystra-Lantz, C., and Shoesmith, C. (2007) TDP43 is a human low molecular weight neurofilament (hNFL) mRNA-binding protein. *Mol. Cell Neurosci.* **35,** 320–327
14. Buratti, E., De Conti, L., Stuani, C., Romano, M., Baralle, M., and Baralle, F. (2010) Nuclear factor TDP-43 can affect selected microRNA levels. *FEBS J.* **277,** 2268–2281
15. Colombrita, C., Zennaro, E., Fallini, C., Weber, M., Sommacal, A., Buratti, E., Silani, V., and Ratti, A. (2009) TDP-43 is recruited to stress granules in conditions of oxidative insult. *J. Neurochem.* **111,** 1051–1061
16. Freibaum, B. D., Chitta, R. K., High, A. A., and Taylor, J. P. (2010) Global analysis of TDP-43 interacting proteins reveals strong association with RNA splicing and translation machinery. *J. Proteome Res.* **9,** 1104–1120
17. Neumann, M., Sampathu, D. M., Kwong, L. K., Truax, A. C., Micsenyi, M. C., Chou, T. T., Bruce, J., Schuck, T., Grossman, M., Clark, C. M., McCluskey, L. F., Miller, B. L., Masliah, E., Mackenzie, I. R., Feldman, H., Feiden, W., Kretzschmar, H. A., Trojanowski, J. Q., and Lee, V. M. (2006) Ubiquitinated TDP-43 in frontotemporal lobar degeneration and amyotrophic lateral sclerosis. *Science* **314,** 130–133
18. Arai, T., Hasegawa, M., Akiyama, H., Ikeda, K., Nonaka, T., Mori, H., Mann, D., Tsuchiya, K., Yoshida, M., Hashizume, Y., and Oda, T. (2006) TDP-43 is a component of ubiquitin-positive tau-negative inclusions in frontotemporal lobar degeneration and amyotrophic lateral sclerosis. *Biochem. Biophys. Res. Commun.* **351,** 602–611
19. Gendron, T. F., Josephs, K. A., and Petrucelli, L. (2010) Review: transactive response DNA-binding protein 43 (TDP-43): mechanisms of neurodegeneration. *Neuropathol. Appl. Neurobiol.* **36,** 97–112
20. Geser, F., Lee, V. M., and Trojanowski, J. Q. (2010) Amyotrophic lateral sclerosis and frontotemporal lobar degeneration: a spectrum of TDP-43 proteinopathies. *Neuropathology* **30,** 103–112
21. Lagier-Tourenne, C., Polymenidou, M., and Cleveland, D. W. (2010) TDP-43 and FUS/TLS: emerging roles in RNA processing and neurodegeneration. *Hum. Mol. Genet.* **19,** R46–64
22. Thorpe, J. R., Tang, H., Atherton, J., and Cairns, N. J. (2008) Fine structural analysis of the neuronal inclusions of frontotemporal lobar degeneration with TDP-43 proteinopathy. *J. Neural. Transmission* **115,** 1661–1671
23. Cairns, N. J., Neumann, M., Bigio, E. H., Holm, I. E., Troost, D., Hatanpaa, K. J., Foong, C., White, C. L., 3rd, Schneider, J. A., Kretzschmar, H. A., Carter, D., Taylor-Reinwald, L., Paulsmeyer, K., Strider, J., Gitcho, M., Goate, A. M., Morris, J. C., Mishra, M., Kwong, L. K., Stieber, A., Xu, Y., Forman, M. S., Trojanowski, J. Q., Lee, V. M., and Mackenzie, I. R. (2007) TDP-43 in familial and sporadic frontotemporal lobar degeneration with ubiquitin inclusions. *Am. J. Pathol.* **171,** 227–240
24. Igaz, L. M., Kwong, L. K., Chen-Plotkin, A., Winton, M. J., Unger, T. L., Xu, Y., Neumann, M., Trojanowski, J. Q., and Lee, V. M. (2009) Expression of TDP-43 C-terminal Fragments *in Vitro* Recapitulates Pathological Features of TDP-43 Proteinopathies. *J. Biol. Chem.* **284,** 8516–8524
25. Zhang, Y. J., Xu, Y. F., Cook, C., Gendron, T. F., Roettges, P., Link, C. D., Lin, W. L., Tong, J., Castanedes-Casey, M., Ash, P., Gass, J., Rangachari, V., Buratti, E., Baralle, F., Golde, T. E., Dickson, D. W., and Petrucelli, L. (2009) Aberrant cleavage of TDP-43 enhances aggregation and cellular toxicity. *Proc. Natl. Acad. Sci. U.S.A.* **106,** 7607–7612
26. Johnson, B. S., McCaffery, J. M., Lindquist, S., and Gitler, A. D. (2008) A yeast TDP-43 proteinopathy model: Exploring the molecular determinants of TDP-43 aggregation and cellular toxicity. *Proc. Natl. Acad. Sci. U.S.A.* **105,** 6439–6444
27. Wils, H., Kleinberger, G., Janssens, J., Pereson, S., Joris, G., Cuijt, I., Smits, V., Ceuterick-de Groote, C., Van Broeckhoven, C., and Kumar-Singh, S. (2010) TDP-43 transgenic mice develop spastic paralysis and neuronal inclusions characteristic of ALS and frontotemporal lobar degeneration. *Proc. Natl. Acad. Sci. U.S.A.* **107,** 3858–3863
28. Krecic, A. M., and Swanson, M. S. (1999) hnRNP complexes: composition, structure, and function. *Curr. Opin. Cell Biol.* **11,** 363–371
29. Shiina, Y., Arima, K., Tabunoki, H., and Satoh, J. (2010) TDP-43 dimerizes in human cells in culture. *Cell. Mol. Neurobiol.* **30,** 641–652
30. Buratti, E., and Baralle, F. E. (2001) Characterization and functional implications of the RNA binding properties of nuclear factor TDP-43, a novel splicing regulator of CFTR exon 9. *J. Biol. Chem.* **276,** 36337–36343
31. Kuo, P. H., Doudeva, L. G., Wang, Y. T., Shen, C. K., and Yuan, H. S. (2009) Structural insights into TDP-43 in nucleic-acid binding and domain interactions. *Nucleic Acids Res.* **37,** 1799–1808
32. Johnson, B. S., Snead, D., Lee, J. J., McCaffery, J. M., Shorter, J., and Gitler, A. D. (2009) TDP-43 is intrinsically aggregation-prone, and amyotrophic lateral sclerosis-linked mutations accelerate aggregation and increase toxicity. *J. Biol. Chem.* **284,** 20329–20339
33. Kabashi, E., Valdmanis, P. N., Dion, P., Spiegelman, D., McConkey, B. J., Vande Velde, C., Bouchard, J. P., Lacomblez, L., Pochigaeva, K., Salachas, F., Pradat, P. F., Camu, W., Meininger, V., Dupre, N., and Rouleau, G. A. (2008) TARDBP mutations in individuals with sporadic and familial amyotrophic lateral sclerosis. *Nat. Genet.* **40,** 572–574
34. Chen, A. K., Lin, R. Y., Hsieh, E. Z., Tu, P. H., Chen, R. P., Liao, T. Y., Chen, W., Wang, C. H., and Huang, J. J. (2010) Induction of amyloid fibrils by the C-terminal fragments of TDP-43 in amyotrophic lateral sclerosis. *J. Am. Chem. Soc.* **132,** 1186–1187
35. Yang, C., Tan, W., Whittle, C., Qiu, L., Cao, L., Akbarian, S., and Xu, Z. (2010) The C-terminal TDP-43 fragments have a high aggregation propensity and harm neurons by a dominant-negative mechanism. *PLoS One* **5,** e15878
36. Li, H. Y., Yeh, P. A., Chiu, H. C., Tang, C. Y., and Tu, B. P. (2011) Hyperphosphorylation as a defense mechanism to reduce TDP-43 aggregation. *PLoS One* **6,** e23075
37. Zhang, Y. J., Xu, Y. F., Dickey, C. A., Buratti, E., Baralle, F., Bailey, R., Pickering-Brown, S., Dickson, D., and Petrucelli, L. (2007) Progranulin mediates caspase-dependent cleavage of TAR DNA binding protein-43. *J. Neurosci.* **27,** 10530–10534
38. Dormann, D., Capell, A., Carlson, A. M., Shankaran, S. S., Rodde, R., Neumann, M., Kremmer, E., Matsuwaki, T., Yamanouchi, K., Nishihara, M., and Haass, C. (2009) Proteolytic processing of TAR DNA binding protein-43 by caspases produces C-terminal fragments with disease defining properties independent of progranulin. *J. Neurochem.* **110,** 1082–1094
39. Nishimoto, Y., Ito, D., Yagi, T., Nihei, Y., Tsunoda, Y., and Suzuki, N. (2010) Characterization of alternative isoforms and inclusion body of the TAR DNA-binding protein-43. *J. Biol. Chem.* **285,** 608–619
40. Chiti, F., and Dobson, C. M. (2006) Protein misfolding, functional amyloid, and human disease. *Annu. Rev. Biochem.* **75,** 333–366
41. Nelson, R., and Eisenberg, D. (2006) Recent atomic models of amyloid fibril structure. *Curr. Opin. Struct. Biol.* **16,** 260–265
42. Petoukhov, M. V., Franke, D., Shkumatov, A. V., Tria, G., Kikhney, A. G., Gajda, M., Gorba, C., Mertens, H. D. T., Konarev, P. V., and Svergun, D. I. (2012) New developments in the ATSAS program package for small-angle scattering data analysis. *J. Appl. Crystallogr.* **45,** 342–350
43. Konarev, P. V., Volkov, V. V., Sokolova, A. V., Koch, M. H., and Svergun,

D. I. (2003) PRIMUS: a Windows PC-based system for small-angle scattering data analysis. *J. Appl. Crystallogr.* **36,** 1277–1282
44. Svergun, D. I. (1992) Determination of the regularization parameter in indirect-transform methods using perceptual criteria. *J. Appl. Crystallogr.* **25,** 495–503
45. Svergun, D. I. (1999) Restoring low resolution structure of biological macromolecules from solution scattering using simulated annealing. *Biophys. J.* **76,** 2879–2886
46. Svergun, D. I., Petoukhov, M. V., and Koch, M. H. (2001) Determination of domain structure of proteins from X-ray solution scattering. *Biophys. J.* **80,** 2946–2953
47. Chen, Y. R., and Glabe, C. G. (2006) Distinct early folding and aggregation properties of Alzheimer amyloid-β peptides Aβ40 and Aβ42: stable trimer or tetramer formation by Aβ42. *J. Biol. Chem.* **281,** 24414–24422
48. Safar, J., Roller, P. P., Gajdusek, D. C., and Gibbs, C. J., Jr. (1993) Thermal stability and conformational transitions of scrapie amyloid (prion) protein correlate with infectivity. *Protein Sci.* **2,** 2206–2216
49. Maurer-Stroh, S., Debulpaep, M., Kuemmerer, N., Lopez de la Paz, M., Martins, I. C., Reumers, J., Morris, K. L., Copland, A., Serpell, L., Serrano, L., Schymkowitz, J. W., and Rousseau, F. (2010) Exploring the sequence determinants of amyloid structure using position-specific scoring matrices. *Nat. Methods* **7,** 237–242
50. Neumann, M. (2009) Molecular neuropathology of TDP-43 proteinopathies. *Int. J. Mol. Sci.* **10,** 232–246
51. Naiki, H., Higuchi, K., Hosokawa, M., and Takeda, T. (1989) Fluorometric determination of amyloid fibrils *in vitro* using the fluorescent dye, thioflavin T1. *Anal. Biochem.* **177,** 244–249
52. Xu, R. M., Jokhan, L., Cheng, X., Mayeda, A., and Krainer, A. R. (1997) Crystal structure of human UP1, the domain of hnRNP A1 that contains two RNA-recognition motifs. *Structure* **5,** 559–570
53. Cléry, A., Blatter, M., and Allain, F. H. (2008) RNA recognition motifs: boring? Not quite. *Curr. Opin. Struct. Biol.* **18,** 290–298
54. Tollervey, J. R., Curk, T., Rogelj, B., Briese, M., Cereda, M., Kayikci, M., König, J., Hortobágyi, T., Nishimura, A. L., Zupunski, V., Patani, R., Chandran, S., Rot, G., Zupan, B., Shaw, C. E., and Ule, J. (2011) Characterizing the RNA targets and position-dependent splicing regulation by TDP-43. *Nat. Neurosci.* **14,** 452–458
55. Polymenidou, M., Lagier-Tourenne, C., Hutt, K. R., Huelga, S. C., Moran, J., Liang, T. Y., Ling, S. C., Sun, E., Wancewicz, E., Mazur, C., Kordasiewicz, H., Sedaghat, Y., Donohue, J. P., Shiue, L., Bennett, C. F., Yeo, G. W., and Cleveland, D. W. (2011) Brain glucosensing and the K(ATP) channel. *Nat. Neurosci.* **14,** 459–468
56. Nonaka, T., Kametani, F., Arai, T., Akiyama, H., and Hasegawa, M. (2009) Truncation and pathogenic mutations facilitate the formation of intracellular aggregates of TDP-43. *Hum. Mol. Genet.* **18,** 3353–3364
57. Winton, M. J., Igaz, L. M., Wong, M. M., Kwong, L. K., Trojanowski, J. Q., and Lee, V. M. (2008) Disturbance of nuclear and cytoplasmic TAR DNA-binding protein (TDP-43) induces disease-like redistribution, sequestration, and aggregate formation. *J. Biol. Chem.* **283,** 13302–13309
58. Stromer, T., and Serpell, L. C. (2005) Structure and morphology of the Alzheimer's amyloid fibril. *Microsc. Res. Tech.* **67,** 210–217
59. Cohen, T. J., Hwang, A. W., Unger, T., Trojanowski, J. Q., and Lee, V. M. (2012) Redox signalling directly regulates TDP-43 via cysteine oxidation and disulphide cross-linking. *EMBO J.* **31,** 1241–1252
60. Pesiridis, G. S., Tripathy, K., Tanik, S., Trojanowski, J. Q., and Lee, V. M. (2011) A "two-hit" hypothesis for inclusion formation by carboxyl-terminal fragments of TDP-43 protein linked to RNA depletion and impaired microtubule-dependent transport. *J. Biol. Chem.* **286,** 18845–18855